Accepted Manuscript

Title: Analysis of Contaminated Nuclear Plant Steel by Laser-Induced Breakdown Spectroscopy

Authors: Adam Lang, Dirk Engelberg, Nicholas T. Smith, Divyesh Trivedi, Owen Horsfall, Anthony Banford, Philip A. Martin, Paul Coffey, William R. Bower, Clemens Walther, Martin Weiß, Hauke Bosco, Alex Jenkins, Gareth T.W. Law

PII: S0304-3894(17)30819-1
DOI: https://doi.org/10.1016/j.jhazmat.2017.10.064
Reference: HAZMAT 18969

To appear in: *Journal of Hazardous Materials*

Received date: 24-4-2017
Revised date: 30-10-2017
Accepted date: 31-10-2017

Please cite this article as: Adam Lang, Dirk Engelberg, Nicholas T.Smith, Divyesh Trivedi, Owen Horsfall, Anthony Banford, Philip A.Martin, Paul Coffey, William R.Bower, Clemens Walther, Martin Weiß, Hauke Bosco, Alex Jenkins, Gareth T.W.Law, Analysis of Contaminated Nuclear Plant Steel by Laser-Induced Breakdown Spectroscopy, Journal of Hazardous Materials https://doi.org/10.1016/j.jhazmat.2017.10.064

Analysis of Contaminated Nuclear Plant Steel by Laser-Induced Breakdown Spectroscopy

Adam Lang[a,b], Dirk Engelberg[b], Nicholas T. Smith[c,d,e], Divyesh Trivedi[c,e], Owen Horsfall[c,e], Anthony Banford[c,e], Philip A. Martin[e], Paul Coffey[e], William R. Bower[a], Clemens Walther[f], Martin Weiß[f], Hauke Bosco[f], Alex Jenkins[g], and Gareth T. W. Law[a,*]

[a]Centre for Radiochemistry Research, School of Chemistry, The University of Manchester, Oxford Road, Manchester, M13 9PL, United Kingdom.

[b]Corrosion and Protection Centre, Materials Performance Centre, School of Materials, The University of Manchester, Oxford Road, Manchester, M13 9PL, United Kingdom.

[c]National Nuclear Laboratory, Chadwick House, Warrington Road, Birchwood Park, Warrington, WA3 6AE, United Kingdom.

[d]School of Earth and Environmental Sciences, The University of Manchester, Oxford Road, Manchester, M13 9PL, United Kingdom.

[e]School of Chemical Engineering and Analytical Sciences, The University of Manchester, Oxford Road, Manchester, M13 9PL, United Kingdom.

[f]Institute for Radioecology and Radiation Protection, Leibniz-Universität Hannover, Herrenhäuser Straße 2, D-30419 Hannover, Germany.

[g]Decontamination Centre of Expertise, B582 Ground Floor North, Sellafield Ltd., Sellafield, Cumbria, CA20 1PG, United Kingdom.

* Telephone: +44 (0) 161 306 0514; Email: gareth.law@manchester.ac.uk; Fax: +44 (0) 161 275 4598

Highlights

- Standoff LIBS analysis of Sr and Cs contaminated nuclear plant steel is demonstrated at millimetre distances.
- Standoff LIBS has the potential to allow surveying of contamination at much larger distances (metres).
- Multi pulse LIBS can also provide depth resolved information on contaminant distribution in steel.

Abstract

Laser Induced Breakdown Spectroscopy (LIBS) has the potential to allow direct, standoff measurement of contaminants on nuclear plant. Here, LIBS is evaluated as an analytical tool for measurement of Sr and Cs contamination on type 304 stainless steel surfaces. Samples were

reacted in model acidic (PUREX reprocessing) and alkaline (spent fuel ponds) Sr and Cs bearing liquors, with LIBS multi-pulse ablation also explored to measure contaminant penetration. The Sr II (407.77 nm) and Cs I (894.35 nm) emission lines could be separated from the bulk emission spectra, though only Sr could be reliably detected at surface loadings > 0.5 mg cm^{-2}. Depth profiling showed decay of the Sr signal with time, but importantly, elemental analysis indicated that material expelled from LIBS craters is redistributed and may interfere in later laser shot analyses.

Keywords: LIBS; contaminated stainless steel; decommissioning; strontium; cesium.

1. Introduction

Laser Induced Breakdown Spectroscopy (LIBS) is a quasi-non-destructive technique that operates on the fundamental principle of the ablation of a small amount of sample by a laser pulse that is focused onto the surface. The ablated material then forms a plasma of excited atoms, ions, and free electrons that, on cooling, emits radiation at characteristic wavelengths dependent upon the elemental composition of the sample. Increasingly, LIBS is being recognised as a promising technique for elemental analysis, including in industry [1]. Examples of use include: elemental analysis in space exploration programs [2], quality control use in pharmaceuticals [3], and forensic and archaeological sample analysis [4]. This diverse range of LIBS applications is largely driven by the technique's capability to perform fast, multi-elemental analysis of solids [5], liquids [6], and gases [7], with virtually no sample preparation, and with low ppm sensitivity.

LIBS is also used in the nuclear industry as the technique permits standoff analysis of radioactive samples at millimetre to 10's of metres of distance. Therein, a rapidly emerging application is elemental analysis of radioactive waste processing materials for the assessment of radionuclide contamination. Positive identification of fission products, actinides, and activated corrosion products has been demonstrated for a range of nuclear materials, including mixed oxide fuels [8], molten salt electrolytes [9], and graphite [10]. LIBS has also been used for analysis of nuclear plant steels; however, work here has focused on analysis of steel alloying components for quality control during manufacturing [11-12], or for discrimination between different kinds of steel for the rapid identification and sorting of unknown materials [13-14]. To our knowledge, LIBS has not been used to quantify radionuclide uptake onto steel components.

The radioactive contamination of steel components is a key decommissioning challenge at nuclear reprocessing facilities [15]. Deposition of radionuclides from reprocessing streams onto steel components incurs a radiation dose to nearby workers and, if left untreated, can generate large volumes of radioactive waste. In turn, these wastes are difficult and costly to characterise, dispose, or decontaminate. It is therefore highly desirable to develop analytical techniques that permit rapid, standoff assessment of contaminated plant components in order to limit human exposure and to allow evaluation of materials needing decontamination and/or sentencing whilst also minimising dose to on-site workers as they can operate LIBS equipment away from the material being analysed. LIBS presents an attractive option to meet this task as it only requires optical access to samples. Accordingly, analysis may be completed in radiologically and chemically hazardous areas such as hot cells without incurring an additional dose penalty. This is in sharp contrast to wet techniques currently employed for the quantitative analysis of nuclear materials [16-17] which by comparison require comparatively long analysis times. Further, these methods are often commercially expensive and hence not economically suited for the analysis of industrial volumes of material. Such issues are overcome with LIBS, which can perform real-time quantitative analysis of multiple elements with minimal restrictions on sample condition. An additional possibility of LIBS is its potential to perform high-resolution depth profiling of materials by multi-pulse laser excitation [1]. In turn, this could yield useful information of contaminant penetration into nuclear plant steels or other contaminated materials.

For successful application of LIBS to nuclear plant steels, the discrimination of analyte emission lines from the supporting matrix spectrum must be possible. The large number of alloying elements typically present in steel reduces this probability of satisfying this prerequisite condition. However, in this contribution we evaluate the ability of LIBS to reliably measure strontium and cesium contamination in AISI Type 304 stainless steel, a common construction material used throughout nuclear reprocessing facilities owing to its excellent corrosion resistance properties [18]. The selection of these two elements reflects the dominant contribution of the fission products ^{90}Sr ($t_{1/2}$ = 28.8 yrs) and ^{137}Cs ($t_{1/2}$ = 30.2 yrs) to the total initial (< 200 years) activity of spent fuel (and resulting spent fuel reprocessing liquors and storage pond waters) after removal from reactors [19]. In addition, we also assess the potential of LIBS to be used as a depth profiling technique for Sr and Cs penetration into steels using LIBS multi-pulse analysis over a single position, as previously documented for other materials [20-21].

2. Experimental

2.1. Steel Samples

The chemical composition of the AISI Type 304 stainless steel used in experiments is provided in Table 1. Steel coupons with dimensions of 10 x 10 x 13 mm (l x w x h) were mechanically polished to 4000 grit using SiC paper on a single 10 x 10 mm face. This surface was then polished to 1 µm mirror finish and degreased with ethanol before contamination experiments commenced. The polished finish was necessary for later TOF-SIMS and GD-OES analysis (see below), and it is important to note that the polished surface has no impact on LIBS measurements. The coupons were then exposed to the contaminant bearing liquors, either 3 M HNO_3, representative of the PUREX-derived nitric acid reprocessing liquors [22], or 1 mM NaOH, representative of alkaline fuel ponds at Sellafield Ltd. site. Aristar grade chemicals were used, and only the polished steel surface was exposed to the aqueous solutions that also contained stable cesium (500 mg L^{-1}) and strontium (500 mg L^{-1}). Contamination experiments were maintained at 60 °C for 30 days; thereafter the coupons were removed and washed briefly with deionised water and then isopropyl alcohol (IPA) prior to LIBS analysis. Solution analysis (Inductively Coupled Plasma Mass Spectrometry) revealed that the total amount of strontium deposited onto the steel surfaces after acidic and alkaline contamination was 0.48 and 1.10 mg cm^{-2}, respectively. In comparison, cesium accumulation was 0.51 and 0.56 mg cm^{-2}, respectively.

Table 1. Chemical Composition (wt. %) of AISI Type 304 Stainless steel used in experiments.

Cr	**Ni**	**C**	**Mn**	**Si**	**P**	**S**	**N**	**Fe**
18.15	8.6	0.055	1.38	0.45	0.04	0.005	0.038	Bal.

2.2. LIBS Analysis

A Q-switched Nd:YAG pulsed laser (10 Hz EKSPLA Nanosecond E/O laser model NL301G-10; fundamental wavelength of 1064 nm) was used in this study. A scheme of the instrument is provided in the Supporting Information. The laser pulse energy was set to 100 mJ, a starting energy that was proven to be useful, and was later adjusted as required. The temporal laser beam width was 3-6 ns, and the repetition rate between successive laser pulses was fixed at 10 Hz. The light emitted from the cooling plasma was collected by a plano-convex quartz lens with focal length of 75 mm into the entrance slit of a 0.5 m focal length Fiber Optic Spectrometer (AvaSpec-2048-USB2-APL27), equipped with indexable gratings of 1200, 2400, and 3600

grooves mm^{-1}, respectively. The dispersed plasma light was detected using a charge coupled device (CCD) detector (2048 pixel) with controls to enable setting the delay and integration time. An emission spectrum within the region 185 - 904 nm was generated from a single laser shot, which permitted identification of the necessary elements through their unique spectral features. Full width at half maximum for the spectrometer was a minimum of 0.03nm across the spectral range. The gate-width was 1.1 ms and the delay time for analysis was fixed at the minimum value of 1.27 µs, a standard time delay. Detector and plasma parameters are presented in the Supporting Information.

2.3. Glow Discharge Optical Emission Spectroscopy Depth Analysis

Elemental depth profile analysis was conducted with GD-OES (Glow Discharge Optical Emission Spectroscopy), using a GD-Profiler 2 (Horiba Jobin Yvon) at an applied power of 35 W and an Ar gas pressure of 635 Pa. A 4 mm diameter Cu anode was used. The elemental emission lines used were 371.999 nm for Fe, 425.439 nm for Cr, 341.482 nm for Ni, 130.223 nm for O, 460.739 nm for Sr, 455.329 nm for Cs, and 396.157 nm for Al. These lines were detected using a polychromator focal length of 500 mm and with 30 optical windows. The photon detector was calibrated using a 1 mm Al sheet. In order to maintain the vacuum seal at the O-ring-sample interface, larger, analogue steel coupons of dimensions 20 mm x 20 mm x 13 mm thickness were used for GD-OES analysis.

2.4. Electron Microscopy and Energy Dispersive X-ray Elemental Analysis

To determine the morphology of the steel surface after the ablation process, SEM analysis was undertaken on the resulting craters that formed upon laser impact. Electron microscopy images were obtained using a FEI XL30 200 (E)SEM-FEG microscope at an accelerating voltage of 15 keV under high vacuum, utilising either an Everhart-Thornley detector (ETD) or a Circular Backscatter detector (CBS). An EDAX Gemeni EDS Spectrometer was used to determine the distribution of major elements (Fe, Cr, Ni, O) on the steel surface at a spot size of approximately 1µm.

2.5. Laser Confocal Microscopy Analysis

The morphology and depth of craters that resulted from LIBS analysis of steel surfaces were analysed with a Keyence VK-X200K 3D laser confocal microscope at 200x magnification using a 0.5 µm step size and superfine resolution (2048 x 1536 pixels). The area analysed by the laser confocal microscopy of the LIBS crater was approximately 2.0 mm x 1.5 mm.

2.6. Time of Flight Secondary Ion Mass Spectrometry

Elemental distribution of the LIBS crater (including Sr and Cs) was analysed using a TOF-SIMS instrument (IONTOF GmbH, Münster, Germany) of the reflectron-type. The system was equipped with a 30 kV Bi/Mn liquid metal ion gun (LMIG) as the primary ion source and was operated at an emission current of 0.8 µA. The pulse width of the bunched primary ion pulse was set to 30 ns at a 100 µs cycle time, which yielded a mass resolution of secondary ions >8000 amu. Prior to analysis, in situ sputter cleaning of the surface was undertaken with an argon gas cluster ion beam (GCIB) in order to remove surface bound hydrocarbon contamination. The scanning area of the LIBS crater was set to 500 µm x 500 µm, the maximum area size for high resolution imaging. The major isotopes of the elements of interest were selected for analysis.

3. Results and Discussion

3.1. Strontium Identification

Initially, strontium and cesium emission lines were identified within the LIBS spectrum of contaminated coupons. A fraction of the underlying stainless steel support matrix is also ablated in tandem with the target elements, and therefore lines corresponding to elements in the substrate will also be observed in the emission spectrum. For this reason the possibility of spectral interference must be considered when selecting analyte lines for positive elemental identification. In contrast to many previous LIBS investigations of nuclear materials, the 304 stainless steel matrix comprises a large number of alloying elements and thus it yields a complex LIBS spectrum, irrespective of the surrounding atmosphere, as shown in Figure 1. The number of strontium and cesium spectral features that are free of interference can be expected to be low within the spectrum of stainless steel due to its multi-element composition. Accordingly, the choice of elemental line for positive detection must be carefully considered as those employed for other materials may not be suitable on the steel matrix.

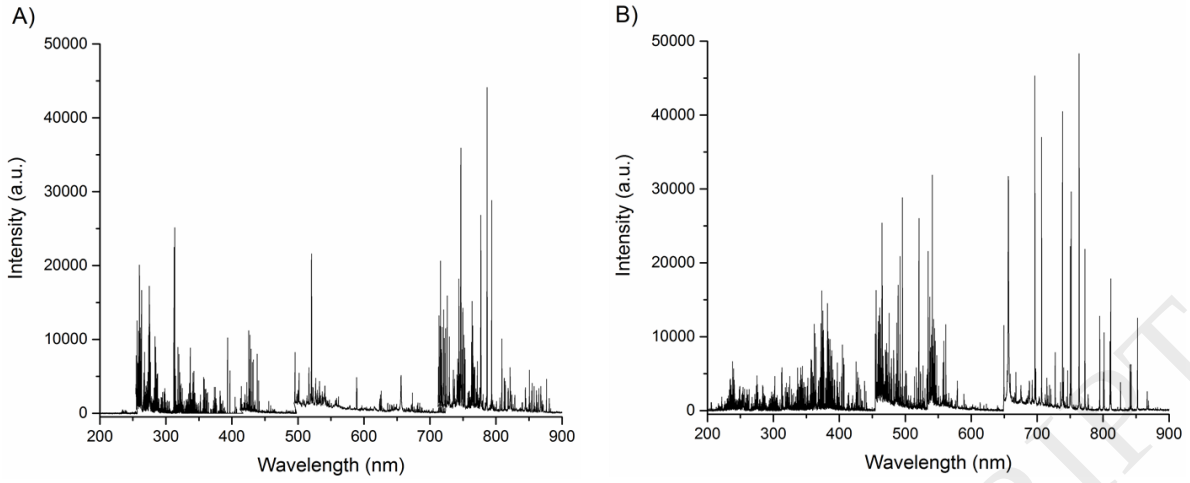

Figure 1. LIBS emission spectra for 'as received' AISI Type 304 stainless steel under air (A) and argon (B) atmospheres.

Previous research has used 407.77 nm for Sr measurement (407.77 nm represents Sr II; $^2S_{1/2} \rightarrow {}^2P_{3/2}$) in LIBS experimentation [2, 8, 23-24], and in accordance this emission line was first tested in this work. As shown in Figure 2A, a 407.77 nm spectral line observable in the contaminated material is absent in the reference uncontaminated specimen, suggesting that this is the strontium line that is useful for measurements. Owing to the large number of alloying elements present in the matrix, the LIBS spectra of stainless steel materials are inherently complex and subsequently peak assignment can often be a challenging task. In consideration of this, a LIBS spectrum of a standard strontium salt ($Sr(NO_3)_2$) was also recorded to support our assignment as Sr II 407.77 nm. The nitrate salt was deemed as an appropriate reference strontium material as it was considered that nitrogen and oxygen do not contribute to the signal of interest. This was based on the omission of the 407.77 nm spectral feature in the open air spectrum of the uncontaminated steel material, despite an abundance of N_2 and O_2 in the surrounding atmosphere. Hence, the observation of this line in the salt spectrum validates our designation as Sr II 407.77 nm and strongly suggests that the steel alloying elements also do not contribute to the signal. Therefore, the Sr II 407.77 nm line can be satisfactorily utilised for the positive identification of strontium within the steel matrix.

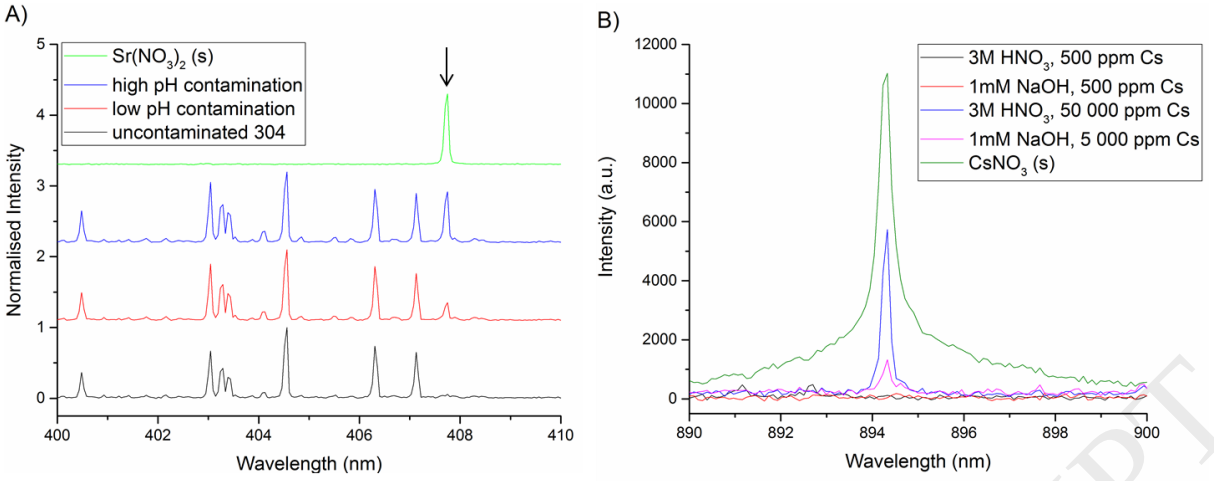

Figure 2. Comparison of LIBS emission spectra in the regions of interest for (A) Sr, and (B) Cs detection. The arrow shows the position of the Sr II 407.77 nm line. Measurement was performed under open air conditions at a laser output energy of 100 mJ. The spectra in (A) were normalised to 1 for ease of comparison.

A comparison of the normalised intensities of the Sr line in the contaminated LIBS spectra reveals uptake to be significantly enhanced in the alkaline contamination matrix, consistent with the ICP-MS solution data. This is also in accordance with previous contamination studies that reported an increasing affinity for metal ion sorption onto steel surfaces in alkaline media [25-26], although no consensus of the mechanisms involved was provided. In order to quantify the observed pH dependence on strontium deposition, construction of calibration curves using standard samples would be necessary to convert signal intensity into concentration [23, 27], which is beyond the scope of this work.

3.2. Cesium Identification

The lack of LIBS investigations in the literature with Cs as the target element has previously been attributed to its poor limit of detection [10], and as a result studies have largely been limited to the analysis of samples where Cs is a major constituent of the substrate [27-28]. Here, the prominent Cs I 852.11 nm line was almost exclusively selected for quantification but in this study interference with the atmospheric (air) Ar I line at 852.14 nm was observed [29] (Supporting Information Figure S3), necessitating the selection of another candidate line. The prominent Cs I 455.53 nm and 459.32 nm lines [30] were discarded for identification purposes on similar grounds as spectral interference with the Cr I 455.48 [31] and Fe I 459.52 nm [32]

matrix lines were observed (Figure 1). The Cs I 894.35 nm line ($^2S_{1/2} \rightarrow {}^2P_{1/2}$) was considered as an appropriate alternative in this work due to its applicability for a number of supporting matrices that have previously been tested [30]. As seen in Figure 2B the LIBS emission spectrum of contaminated 304 includes a line centred at 894.33 nm that is not present in the uncontaminated spectrum. To confirm this, we completed complimentary analysis of $CsNO_3$, and found that the Cs I 894.35 nm line was observed. This line, however, only became visible when the solution concentrations were increased by one to two orders of magnitude in both the alkaline and acidic systems, respectively. No detectable quantities of cesium could be found on the steel surface using contamination solution conditions representative of conditions found at nuclear reprocessing facilities. Hence, the sensitivity of LIBS with regards to Cs detection was not satisfactory in our study [10].

3.3. Chemical Depth Profiling

A fundamental challenge associated with depth profiling techniques is the correlation of analyte removal rate with depth of analysis. LIBS is no exception to this, and currently no established method for depth quantification exists. A relatively simple calibration procedure employed in previous studies involved calculation of the average ablation rate by dividing the thickness of a standard material by the corresponding number of shots required to ablate from top to bottom [21, 33]. Subsequent measurement of crater depth by electron microscopy and stylus profilometry demonstrated this approach to be dubious, by the observation of an obvious non-linear ablation rate [34]. A decreasing ablation rate at greater depths has subsequently been attributed to stronger absorption of the laser pulse by the plasma as it penetrates further into the material, reducing its capacity to remove material upon contact with the crater bottom [35]. Adding to these difficulties is apparent irregular crater morphology where the crater bottom typically does not have a flat surface, thus making it difficult to accurately determine depth by direct measurement [36].

The procedure used to obtain LIBS chemical depth information in this work is described as follows. The spontaneous formation of a passive surface chromium oxide layer on stainless steel materials is exploited in an analogous approach to the aforementioned studies of coated systems, using oxygen as the reference element confined to the surface. Using this approach, the decreasing oxygen signal in the initial pulses corresponds to the ablation of the passive layer and thus can be monitored to evaluate contamination relative to this surface film. To avoid contribution of the LIBS signal by atmospheric oxygen, analysis must be performed under an

inert atmosphere. Many of the plasma properties including size, temperature and expansion rate are strongly influenced by its surrounding atmosphere and therefore the choice of atmosphere must be carefully selected to be complimentary with the nature of analysis. Argon is reported to yield intense spectral lines whilst simultaneously possessing a low surface ablation rate [37], attributed to its low thermal conductivity that subsequently heats the plasma more effectively by inverse Bremsstrahlung. The resulting plasma also acts as a protective barrier, optically shielding the surface and thus reducing the volume of ablation. The combination of intense spectral lines corresponding to smaller volumes of ablated material for each individual shot affords improved depth resolution for chemical analysis and for this reason argon was chosen as the atmosphere for depth profiling analysis in this study.

LIBS depth profiles of Sr and Cs contaminated steel coupons are shown in Figure 3. The capability of LIBS to reliably perform Cs depth characterisation was not considered owing to the challenges involving positive detection under conditions representative of nuclear reprocessing facilities. To overcome poor accuracy, normalization of analyte signals to the Fe I 404.56 nm matrix line was performed; a common practice in elemental analysis [1-2]. In order to demonstrate the validity of this approach, the Cr I emission line at 425.39 nm was also monitored, where the relatively stable signal observed suggests that the assumption of a uniform Fe distribution within the matrix is reasonable. Operating at a laser energy of 100 mJ $shot^{-1}$ reveals a maximum strontium concentration within the initial pulses. However, strong fluctuation in the strontium signal for the alkaline system, where contamination is much more pronounced, makes it unfeasible to accurately evaluate strontium contamination depth. This observation is much less pronounced for a laser energy of 50 mJ $shot^{-1}$, suggesting it to be a consequence of matrix effects intrinsic to the LIBS experimental configuration, rather than a correct reflection of strontium contamination behaviour. In addition, inconsistent oxygen depth profiles were also observed between the acidic and alkaline systems at high laser fluence, where the signal was significantly diminished for the high pH specimen. This effect was not observed at lower laser fluence. A possible explanation for the apparent significance of the laser parameters is addressed later. Measuring at a reduced laser output it also becomes apparent that oxygen persists for at least an equal number of shots as the corresponding strontium signal. This observation now becomes possible only by the smoother decline of the strontium signal in the associated depth profiles. From this result it would seem that strontium is maintained within close proximity to the surface, and does not diffuse into the bulk material.

To check the validity of our proposed method, complimentary depth-resolved analysis of the contaminated steel coupons was undertaken using a commercial GD-OES. The separation of sample removal and excitation processes in glow discharge techniques is a key distinction from LIBS that, in tandem with a stable discharge, is responsible for the reduction of matrix effects. Hence, suitable algorithms are available for the quantification of glow discharge emission yields [38] and for the conversion of sputtering rate to depth information [39]. As a result, GD-OES to date remains a more universal technique for elemental depth analysis, as demonstrated by the widespread investigations reported involving steel materials [40-43].

The GD-OES depth profiles of the steel coupons after contamination are shown in Figure 4. By monitoring the oxygen signal, the interface position was located after a sputtering time of approximately 0.20 and 0.30 seconds for the low and high pH contaminating solutions, respectively. In both instances, strontium enrichment was observed within the Cr_2O_3 passive layer, as indicated by the alignment of the strontium, chromium, and oxygen signal maxima. This finding is consistent with the LIBS result in that contamination diffusion is effectively inhibited by the passive layer. An important distinguishing feature however is the improved depth resolution afforded by the GD-OES technique, which is capable of discriminating between surface complexation and passive layer embedment. This is a clear advantage over LIBS which in this study, is only sufficient to classify contamination as a surface phenomenon. Furthermore, no Cs signal could be detected during GD-OES characterisation, irrespective of contamination conditions. This result further emphasises that optical emission based spectroscopic techniques are currently not sensitive enough for the analysis of cesium [10].

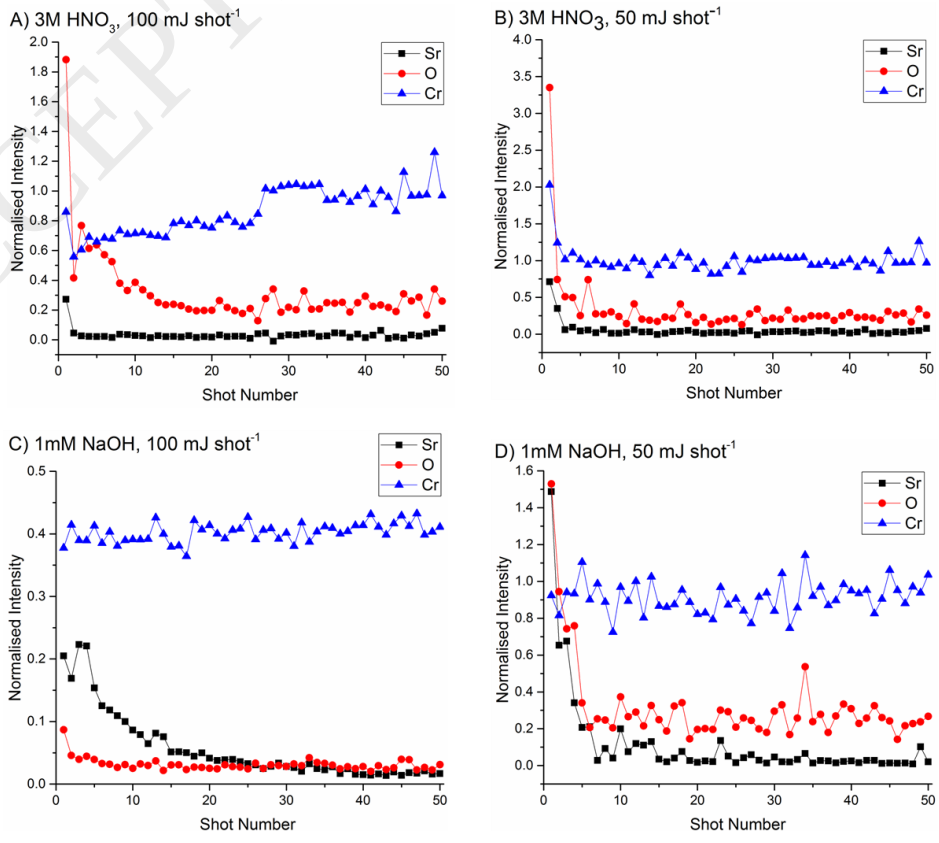

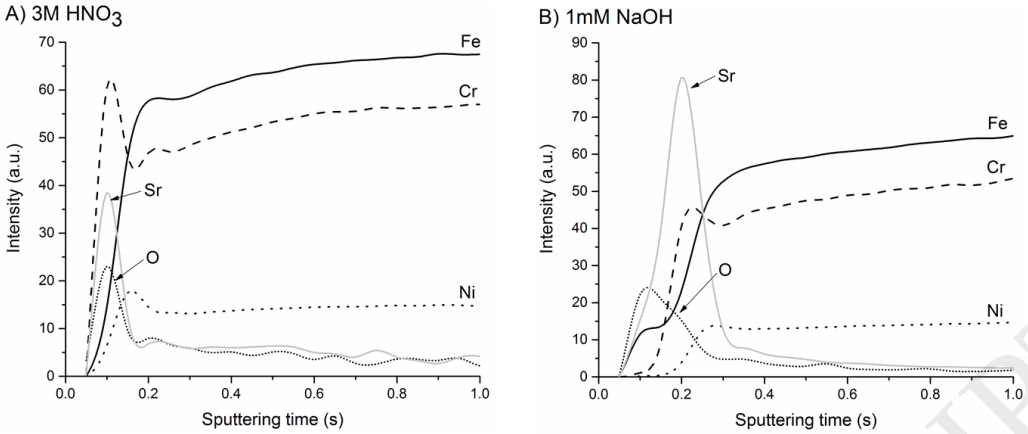

Figure 3. Comparison of LIBS depth profiles measured in an argon environment for acidic and alkaline contaminated stainless steel at 100 mJ and 50 mJ laser energy. The Sr signal in (C) was scaled by a factor of 0.1 for clarity.

Figure 4. GD-OES depth profiles of 304 stainless steel contaminated in 3M HNO_3 and 1mM NaOH. For clarity the Sr signals have been scaled by a factor of 100 for the acidic and alkaline systems.

3.4. Crater Analysis

The analysis of major element distribution (Fe, Cr, O, Ni) around LIBS craters, as a function of total number of laser shots delivered, is shown in Figure 5. In all cases, the craters produced were approximately 1 mm in diameter. The study was carried out using high pH contaminated steel samples using 100 mJ shots in an argon medium because fluctuation of the strontium signal was most evident under these conditions. It can clearly be seen that with an increasing number of shots, a distinct crater geometry develops in which discrete concentric rings of non-uniform elemental composition form. A prominent feature is the increasing oxygen concentration at the crater rim with shot number, which may be attributed to material being expelled from the crater and accumulating around the perimeter as a solidified oxide melt.

The absence of the major steel alloying elements in the melt however suggests that the nature of this laser-matter interaction is not dominated by the relative concentrations of the matrix

elements within the plasma plume. Taking into consideration the irregular Sr and O depth profiles recorded at high laser fluence (Figure 3), it is possible that strontium (which could not be reliably detected by EDX) redistribution processes are also occurring during the LIBS measurement. This was investigated via complementary elemental spatial distribution analysis with TOF-SIMS. The crater surface morphology was also characterised by confocal microscopy to identify potential regions of settled debris. As shown in Figure 6, strontium enrichment is observed both within the central position and around the rim of the crater formed from a single 100 mJ shot. In addition to the depletion of iron, chromium, and nickel, these identifiable regions of strontium deposition are raised above the unablated surface, as demonstrated by the colour coded height map. These results collectively indicate that strontium is also being expelled from the crater and is subsequently returned as a concentrated form of settling debris.

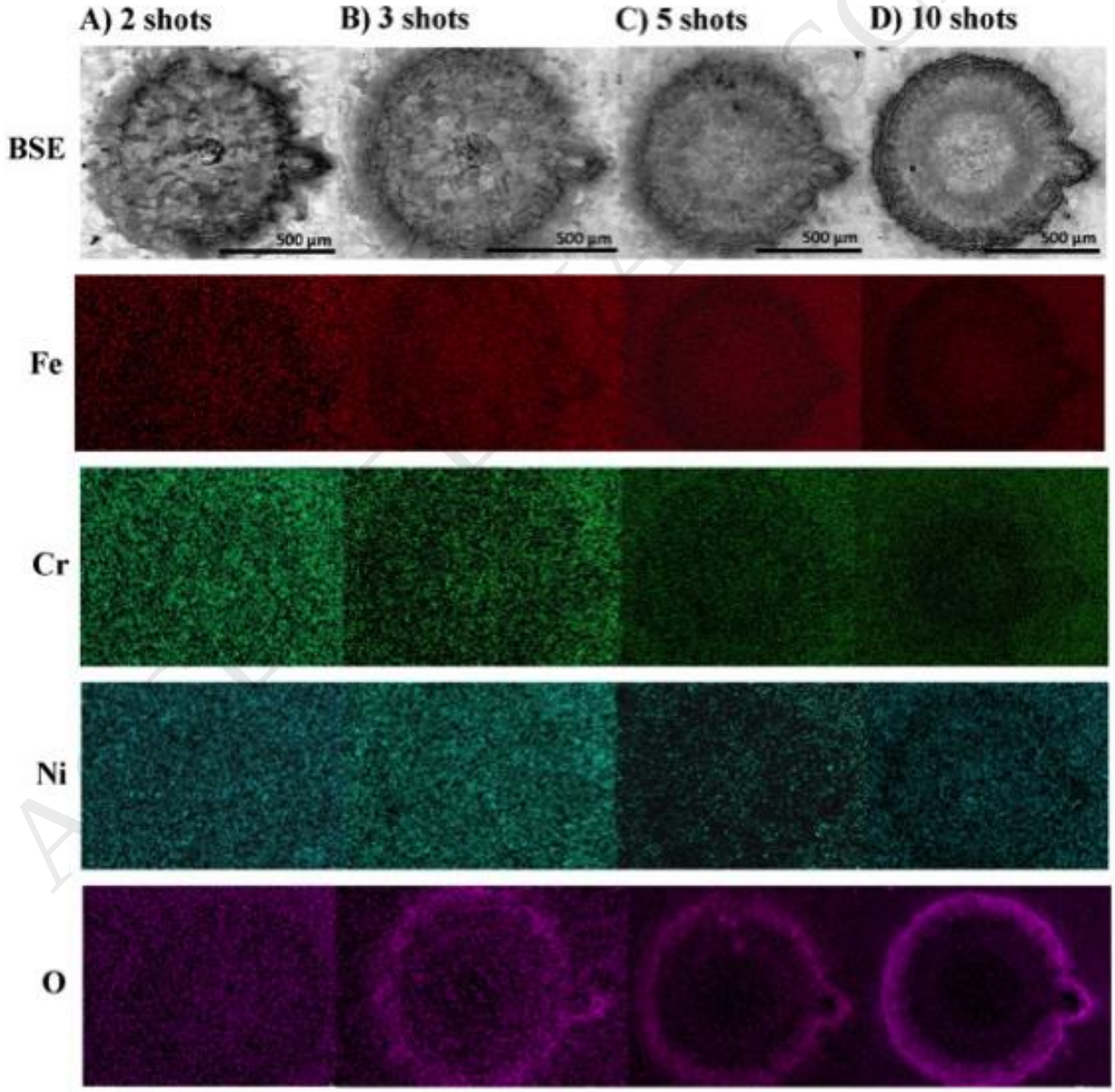

Figure 5. SEM image and SEM-EDX elemental maps of LIBS craters formed on the high pH contaminated steel surface after a different number of 100 mJ shots under argon.

The homogenous distribution of oxygen within the crater is consistent with the EDX result that accumulation of oxide debris is insignificant for a low number of shots. Nevertheless, this result excludes the likelihood of strontium being deposited as SrO, where the exact chemical composition of the debris is subsequently not clear. Regardless, the presence of settled strontium and oxygen material on the specimen surface may subsequently be re-analysed in tandem with ablation of deeper regions, producing a residual tailing of the analyte signals that in turn leads to a compromised depth resolution. This possibility has been considered previously in studies that reported analogous crater morphologies on metallic alloys [44] where in one instance direct observation was possible by electron probe microanalysis [45]. Furthermore, in the

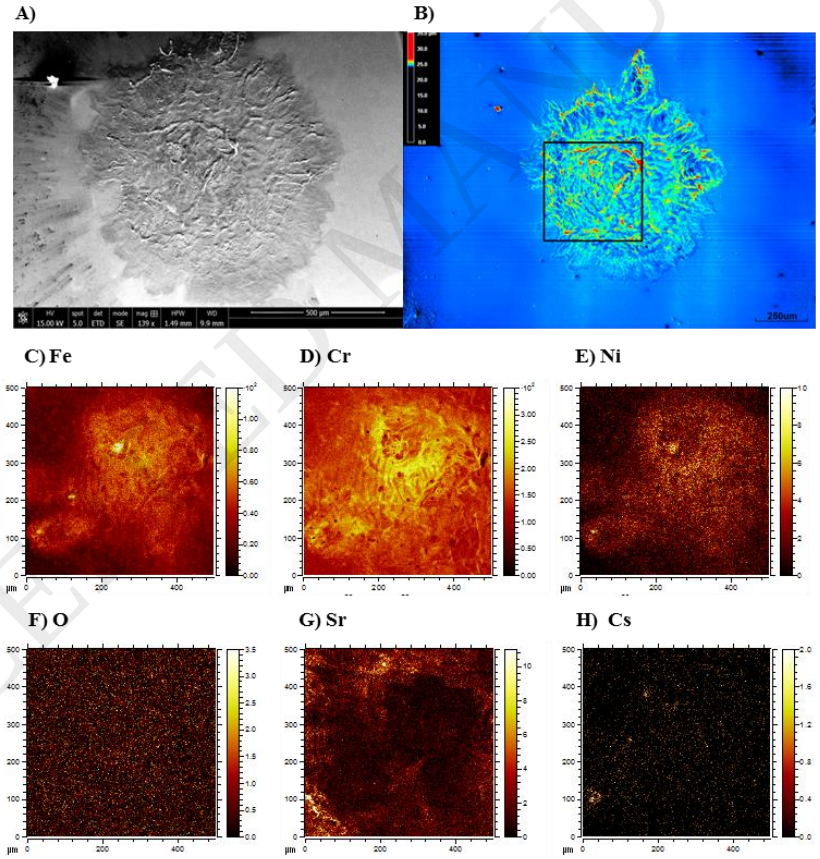

aforementioned studies the severity of the tailing effect was often exacerbated by alterations to experimental parameters that increase laser fluence. This includes tightening the beam focus and reducing working distance, which in turn yielded more irregular crater profiles.

Figure 6. (A) SEM morphology and (B) confocal microscopy analysis of a crater formed on an alkaline contaminated steel sample from a single 100 mJ laser shot under an argon atmosphere. TOF-SIMS elemental analysis of the highlighted region in (B) for the elements (C) Fe, (D) Cr, (E) Ni, (F) O, (G) Sr, and (H) Cs.

It is not the purpose of this paper to explain LIBS crater morphology or its formation in detail, which has been described elsewhere in published literature [46]. Of note, cesium could also be detected with TOF-SIMS (Figure 6) and here the strontium and cesium spatial distribution profiles were also inconsistent, indicating that the redistribution behaviour is unique to each individual element and therefore cannot reliably be inferred from the surface response of another material. A more comprehensive study of crater morphology and evolution is clearly necessary to better understand the surface-laser interaction that is fundamental to LIBS as a characterisation technique. This undertaking is particularly prudent for applications in nuclear decommissioning, since this analysis technique could potentially reintroduce radioactive material onto the material surface.

In addition, it has previously been suggested that laser irradiance treatments may also deteriorate the corrosion resistance of austenitic stainless steels [47]. This behaviour has been attributed to a localised discontinuity of the passive layer under the heating effect of the laser at high fluence [48]. If similar corrosion phenomena are initiated during the LIBS measurement this will present a serious problem for in situ characterisation as a reduced corrosion performance will increase the likelihood of material failure. Further investigation is therefore required to evaluate the effect of the ablation process on the corrosion resistance of stainless steels.

4. Conclusions

We have shown that LIBS can be used to identify Sr and Cs contamination on 304L austenitic stainless steel, a material widely used in the nuclear waste storage and reprocessing operations. Here, the Sr II (407.77 nm) and Cs I (894.35 nm) emission lines can be separated from the overall steel emission spectrum. However, whilst LIBS can reliably measure Sr contamination on steel at levels representative of those found in the nuclear industry (> 0.5 g cm^{-2}), cesium detection at these levels is challenging. LIBS depth profiling of Sr contamination in steel also appears possible; however here, at an output laser energy of 100 mJ $shot^{-1}$ material ablated from the steel surface can be redeposited in the LIBS crater, causing tailing in the Sr signal. Reducing the laser output to 50 mJ $shot^{-1}$ lessens this problem and at this energy LIBS results for Sr depth penetration into steels were in good agreement with complimentary GD-OES analysis. As such,

LIBS offers reliable standoff analysis for Sr contamination in nuclear plant steels at loadings representative of industry. This is an intriguing possibility due to the requirement of minimal sample preparation and handling associated with the LIBS technique. Further, LIBS has the potential to offer real time analysis of contaminant distribution on nuclear plant steel and as such could be used to inform the effectiveness of any contaminant removal technique during decommissioning and plant clean-out.

Acknowledgments

This work was supported by the Sellafield Ltd. Decontamination and Effluents Centre of Expertise and the RCUK grants ST/N002474/1 and NE/M014088/1. Smith is funded by a Royal Society Industry Fellowship, and Banford, Horsfall, Smith and Trivedi acknowledge support from NNL's Waste Management and Decommissioning IR&D Programme.

References

[1] R. Noll, Laser-induced breakdown spectroscopy: Fundamentals and applications, Springer-Verlag, Berlin/Heidelberg, 2012.

[2] A.K. Knight, N.L. Scherbarth, D.A. Cremers, M.J. Ferri, Characterization of laser-induced breakdown spectroscopy (LIBS) for application to space exploration, Appl. Spectrosc. 54 (2000) 331-340.

[3] A.K. Myakalwar, S. Sreedhar, I. Barman, N.C. Dingari, S.V. Rao, P.P. Kiran, S.P. Tewari, G.M. Kumar, Laser-induced breakdown spectroscopy-based investigation and classification of pharmaceutical tablets using multivariate chemometric analysis, Talanta 87 (2011) 53-59.

[4] K. Subedi, T. Trejos, J. Almirall, Forensic analysis of printing inks using tandem Laser induced breakdown spectroscopy and laser ablation inductively coupled plasma mass spectrometry, Spectrochim. Acta B 103-104 (2015) 76-83.

[5] M.V. Belkov, V.S. Burakov, A. De Giacomo, V.V. Kiris, S.N. Raikov, N.V. Tarasenko, Comparison of two laser-induced breakdown spectroscopy techniques for total carbon measurement in soils, Spectrochim. Acta B 64 (2009) 899–904.

[6] D. Alamelu, A. Sarkar, S. Aggrawal, Laser-induced breakdown spectroscopy for simultaneous detection of Sm, Eu and Gd in aqueous solution, Talanta 77 (2008) 256-261.

[7] B. McGann, C.D. Carter, T.M. Ombrello, S. Hammack, T. Lee, H. Do, Gas property measurements in a supersonic combustor using nanosecond gated laser-induced breakdown spectroscopy with direct spectrum matching, Proc. Comb. Inst. 36 (2017) 2857–2864.

[8] P. Fichet, P. Mauchien, C. Moulin, Determination of impurities in uranium and plutonium dioxides by laser-induced breakdown spectroscopy, Appl. Spectrosc. (1999) 1111-1117.

[9] A. Williams, S. Phongikaroon, Laser-induced breakdown spectroscopy (LIBS) in a novel molten salt aerosol system, Appl. Spectrosc. 0 (2016) 1-6.

[10] M. Martin, S. Allman, D. Brice, R. Martin, N. Andre, Exploring laser-induced breakdown spectroscopy for nuclear materials analysis and in-situ applications, Spectrochim. Acta B 74-75 (2012) 177-183.

[11] Z.Z. Wang, Y. Deguchi, F.J. Shou, J.J. Yan, J.P. Liu, Application of laser-induced breakdown spectroscopy to real-time elemental monitoring of iron and steel making processes, ISIJ Int. 56 (2016) 723-735.

[12] J. Liu, Y. Jia, Y. Zhang, N. Sun, Determination of the insoluble aluminium content in steel samples by using laser-induced breakdown spectroscopy, Plasma Sci. Tech. 117 (2015) 644-648.

[13] S. Kashiwakura, K. Wagatsuma, Rapid sorting of stainless steel by open-air laser induced breakdown spectroscopy with detecting chromium, nickel and molybdenum, ISIJ Int. 55 (2015) 2391-2396.

[14] L. Liang, T. Zhang, K. Wang, H. Tang, X. Yang, X. Zhu, Y. Duan, H. Li, Classification of steel materials by laser-induced breakdown spectroscopy coupled with support vector machines, Appl. Optics 53 (2014) 544-552.

[15] International Atomic Agency, Management of spent fuel from nuclear power reactors: Proceedings of an international conference, Vienna, 2006.

[16] Y. Takagi, M. Furukawa, Y. Kamo, K. Suzuki, Sequential inductively coupled plasma quadrupole mass-spectrometric quantification of radioactive strontium-90 incorporating cascade separation steps for radioactive contamination rapid survey, Anal. Methods 6 (2014) 355-362.

[17] E.S.C. Temba, A.S. Reis Júnior, A.M. Amaral, R.P.G. Monteiro, Separation and determination of ^{90}Sr in low-and intermediate level radioactive wastes using extraction chromatography, J. Radioanal. Nucl. Chem. 290 (2011) 631–635.

[18] R. Shaw, Corrosion prevention and control at Sellafield nuclear fuel reprocessing plant, Br. Corros. J. 25 (1990) 97-107.

[19] D. Bodansky, Nuclear Energy, Principles, Practices and Prospects, second ed., Springer, Washington, 2004.

[20] J. Zhang, X. Hu, J. Xi, J. Kong, Z. Ji, Depth profiling of Al diffusion in Si wafers by laser-induced breakdown spectroscopy, J. Anal. At. Spectrom. 28 (2013) 1430-1435.

[21] C.C. Garcia, M. Corral, J.M. Vadillo, J.J. Laserna, Angle-resolved laser-induced breakdown spectrometry for depth profiling of coated materials, Appl. Spectrosc. 54 (2000) 1027-1031.

[22] G.R. Choppin, J. Liljenzin, J. Rydberg, Radiochemistry and Nuclear Chemistry, third ed., Oxford, Elsevier, 2002.

[23] A. Mansoori, B. Roshanzadeh, M. Khalaji, S.H. Tavassoli, Quantitative analysis of cement powder by laser induced breakdown spectroscopy. Opt. Laser Eng. 49 (2011) 318-323.

[24] A.M. Popov, A.N. Drozdova, S.M. Zaytsev, D.I. Biryukova, N.B. Zorov, T.A. Labutin, Rapid, direct determination of strontium in natural waters by laser-induced breakdown spectroscopy, J. Anal. At. Spectrom. 31 (2016) 1123-1130.

[25] S.A. Adeleye, D.A. White, J.B. Taylor, Ambient temperature contamination of process piping and the effects of pretreatment, Nucl. Technol. 113 (1996) 46-53.

[26] P. Dombovári, P. Kádár, T. Kovács, J. Somlai, K. Radó, R. Krisztián, I. Varga, R. Buják, K. Varga, P. Halmos, J. Borszéki, J. Kónya, N.M. Nagy, L. Kövér, D. Varga, I. Cserny, J. Tóth, L. Fodor, A. Horváth, T. Pintér, J. Schunk. Accumulation of uranium on austenitic stainless steel surfaces, Electrochim. Acta 52 (2007) 2542-2451.

[27] A. Metzinger, E. Kovács-Széles, I. Almási, G. Galbács, An assessment of the potential of laser-induced breakdown spectroscopy (LIBS) for the analysis of cesium in liquid samples of biological origin, Appl. Spectrosc. 68 (2014) 789-793.

[28] S.I. Kezawa, M. Wakamatsu, Detection of cesium from pollucite using laser-induced breakdown spectroscopy, Solid State Phenom. 199 (2013) 285-290.

[29] J.B. Shumaker Jr., C.H. Popenoe, Experimental transition probabilities for the Ar I 4s–4p array, J. Opt. Soc. Am. 57 (1967) 8-10.

[30] I. Gaona, J. Serrano, J. Moros, J.J. Laserna, Evaluation of laser-induced breakdown spectroscopy analysis potential for addressing radiological threats from a distance, Spectrochim. Acta B 96 (2014) 12-20.

[31] L. Wallace, K. Hinkle, The 236.6–5400.0 nm Spectrum of Cr I, Astrophys. J. 700 (2009) 720-726.

[32] G. Nave, S. Johansson, R. Learner, A. Thorne, J. Brault, A new multiplet table for Fe I, Astrophys. J., Suppl. Ser. 94 (1994) 221-459.

[33] L. Cabalin, D. Romero, J. Baena, J. Laserna, Saturation effects in the laser ablation of stainless steel in air at atmospheric pressure, Fresenius J. Anal. Chem. 365 (1999) 404-408.

[34] L. St-Onge, M. Sabsabi, Towards quantitative depth-profile analysis using laser-induced plasma spectroscopy: investigation of galvannealed coatings on steel, Spectrochim. Acta B 55 (2000) 299-308.

[35] C. Geertsen, A. Briand, F. Chartier, J. Lacour, P. Mauchien, S. Sjostrom, J. Mermet, Comparison between infrared and ultraviolet-laser ablation at atmospheric pressure-

implications for solid sampling inductively-coupled plasma spectrometry, J. Anal. At. Spectrom. 9 (1994) 17-22.

[36] D. Papazoglou, V. Papadakis, D. Anglos, In situ interferometric depth and topography monitoring in LIBS elemental profiling of multi-layered structures, J. Anal. At. Spectrom. 19 (2004) 483-488.

[37] Y. Ilda, Effects of atmosphere on laser vaporization and excitation processes of solid samples, Spectrochim. Acta B 45 (1990) 1353-1367.

[38] A. Bengtson, T. Nelis, The concept of constant emission yield in GDOES, Anal. Bioanal. Chem. 385 (2006) 568-585.

[39] L. Wilken, V. Hoffmann, K. Wetzig, In situ depth measurements for GD-OES, J. Anal. At. Spectrom. 18 (2003) 1133-40.

[40] N. Fuertes Casals, A. Nazarov, F. Vucko, R. Pettersson, D. Thierryb, Influence of mechanical stress on the potential distribution on a 301 LN stainless steel surface, J. Electrochem. Soc. 162 (2015) C465-C472.

[41] D. Manova, C. Diaz, L. Pichon, G. Abrasonis, S. Mändl, Comparability and accuracy of nitrogen depth profiling in nitride austenitic stainless steel, Nucl. Instrum. Meth. B 349 (2015) 106-113.

[42] E. Marin, A. Lanzutti, M. Lekka, L. Guzman, W. Ensinger, L. Fedrizzi, Chemical and mechanical characterization of TiO_2/Al_2O_3 atomic layer depositions on AISI 316 L stainless steel, Surf. Coat. Tech. 211 (2012) 84-88.

[43] M.G. Shahri, S.R. Hosseini, M. Salehi, M. Naderi, Evaluation of nitrogen diffusion in thermomechanically nanostructured and plasma nitride stainless steel, Surf. Coat. Tech. 296 (2016) 40-45.

[44] L. Cabalin, A. Gonzalez, L. Lazic, J. Laserna, Deep ablation and depth profiling by laser-induced breakdown spectroscopy (LIBS) employing multi-pulse laser excitation: Application to galvanized steel, Appl. Spectrosc. 65 (2011) 797-805.

[45] M. Mateo, M. Vadillo, J. Laserna, Irradiance-dependent depth profiling of layered materials using laser-induced plasma spectrometry, J. Anal. At. Spectrom. 16 (2001) 1317-1321.

[46] B. Lan, M.H. Hong, S.X. Chen, K.D. Ye, Z.B. Wang, G.X. Chen, T.C. Chong, Laser-ablation-induced concentric ring structures, Jpn. J. Appl. Phys. 42 (2003) 5123-5126.

[47] B. Krawczyk, D. Engelberg, Effect of aqua blasting, sandblasting and laser engraving on the corrosion resistance of type 316 stainless steel, BHM. 161 (2016) 50-55.

[48] B. Szubzda, A. Antończak, P. Kozioł,, L. Łazarek, B. Stępak, K. Łęcka, A. Szmaja, M. Ozimej, Corrosion resistance of the AISI 304, 316 and 321 stainless steel surfaces modified by laser, Mater. Sci. Eng. 113 (2016) 1-8.